

Durable SARS-CoV-2 B cell immunity after mild or severe disease

Clinton O. Ogega,¹ Nicole E. Skinner,¹ Paul W. Blair,¹ Han-Sol Park,² Kirsten Littlefield,² Abhinaya Ganesan,² Santosh Dhakal,² Pranay Ladiwala,³ Annukka A.R. Antar,¹ Stuart C. Ray,¹ Michael J. Betenbaugh,³ Andrew Pekosz,² Sabra L. Klein,² Yukari C. Manabe,¹ Andrea L. Cox,^{1,2} and Justin R. Bailey¹

¹Division of Infectious Diseases, Department of Medicine, Johns Hopkins University School of Medicine, Baltimore, Maryland, USA. ²W. Harry Feinstone Department of Molecular Microbiology and Immunology, The Johns Hopkins Bloomberg School of Public Health, Baltimore, Maryland, USA. ³Advanced Mammalian Biomanufacturing Innovation Center, Department of Chemical and Biomolecular Engineering, Johns Hopkins University, Baltimore, Maryland, USA.

Multiple studies have shown loss of severe acute respiratory syndrome coronavirus 2-specific (SARS-CoV-2-specific) antibodies over time after infection, raising concern that humoral immunity against the virus is not durable. If immunity wanes quickly, millions of people may be at risk for reinfection after recovery from coronavirus disease 2019 (COVID-19). However, memory B cells (MBCs) could provide durable humoral immunity even if serum neutralizing antibody titers decline. We performed multidimensional flow cytometric analysis of S protein receptor binding domain-specific (S-RBD-specific) MBCs in cohorts of ambulatory patients with COVID-19 with mild disease ($n = 7$), and hospitalized patients with moderate to severe disease ($n = 7$), at a median of 54 days (range, 39–104 days) after symptom onset. We detected S-RBD-specific class-switched MBCs in 13 of 14 participants, failing only in the individual with the lowest plasma levels of anti-S-RBD IgG and neutralizing antibodies. Resting MBCs (rMBCs) made up the largest proportion of S-RBD-specific MBCs in both cohorts. FCRL5, a marker of functional memory on rMBCs, was more dramatically upregulated on S-RBD-specific rMBCs after mild infection than after severe infection. These data indicate that most SARS-CoV-2-infected individuals develop S-RBD-specific, class-switched rMBCs that resemble germinal center-derived B cells induced by effective vaccination against other pathogens, providing evidence for durable B cell-mediated immunity against SARS-CoV-2 after mild or severe disease.

Introduction

We are in the midst of an ongoing global pandemic caused by a novel coronavirus, severe acute respiratory syndrome coronavirus 2 (SARS-CoV-2). Coronavirus disease 2019 (COVID-19), the disease caused by SARS-CoV-2, can cause pulmonary inflammation, acute respiratory distress syndrome (ARDS), respiratory failure, and death. Despite the high morbidity and mortality caused by COVID-19, the majority of SARS-CoV-2-infected individuals recover and survive (1, 2). Following recovery, the durability of immunity against SARS-CoV-2 remains unclear. Durability of immunity is critical to mitigate the risk of reinfection for millions of people who have recovered or will recover from COVID-19.

After clearance of an infection or effective vaccination, phenotypically distinct B cell populations contribute to short- and long-term humoral immunity. Short-lived antibody-secreting cells (ASCs) in blood and secondary lymphoid organs release antibodies into the circulation for weeks to months. Durable humoral immunity (lasting months to years) is mediated by bone marrow-resident, long-lived ASCs and by memory B cells (MBCs), which rapidly proliferate and differentiate into ASCs in response to antigen rechallenge. Multiple

studies have now demonstrated that serum antibody titers against SARS-CoV-2 wane and can even become undetectable after resolution of infection (3–6), likely reflecting a decline in short-lived ASC populations over time. Although other emerging reports have demonstrated more durable serum antibody responses (7–10), concerns remain that individuals who have recovered from COVID-19 may not maintain adequate immunity against reinfection. Individuals with mild COVID-19 disease generally mount lower titer antibody responses against the virus than those with severe disease (3, 10), raising particular concern that those who recover from mild infection are not protected against reinfection. If present and functional, MBCs could provide durable humoral immunity even after the loss of detectable serum antibody titers, as has been demonstrated after vaccination against viruses like hepatitis B (11, 12). However, Kaneko et al. showed a dramatic loss of germinal centers during acute COVID-19, raising concern that T cell-dependent, durable, class-switched SARS-CoV-2-specific MBC responses may not reliably develop after SARS-CoV-2 infection (13).

Little is known about the frequency and phenotype of SARS-CoV-2-specific MBCs that develop in response to either severe or mild infection. B cells specific for the SARS-CoV-2 Spike (S) protein have been isolated from individuals with very low antibody titers, but the relatively low frequency of these cells has thus far limited further characterization (14). We developed a highly sensitive and specific flow cytometry-based assay to quantitate circulating SARS-CoV-2 S protein receptor binding domain-specific

Conflict of interest: The authors have declared that no conflict of interest exists.

Copyright: © 2021, American Society for Clinical Investigation.

Submitted: October 28, 2020; **Accepted:** February 10, 2021; **Published:** April 1, 2021.

Reference information: *J Clin Invest.* 2021;131(7):e145516.

<https://doi.org/10.1172/JCI145516>.

Table 1. Participant characteristics

Participant ID	Age	Sex	Race	Ethnicity	Days from symptom onset	FLU-PRO ^A	Supplemental O ₂ ^B
Mild, ambulatory							
SE-JH-A-A0006	63	F	White	Non-Hispanic	63	0.38	None
SE-JH-A-A0021	53	F	Hawaiian/Pacific Islander	Non-Hispanic	68	0.28	None
SE-JH-A-A0033	62	F	White	Hispanic	59	0.19	None
SE-JH-A-A0039	71	F	White	Non-Hispanic	64	0.06	None
SE-JH-A-A0046	56	M	White	Non-Hispanic	46	0	None
SE-JH-A-A0054	43	M	Black	Non-Hispanic	61	0.03	None
SE-JH-A-A0060	32	M	American Indian/ Alaska Native	Non-Hispanic	45	0.09	None
Median	56				61	0.09	
Severe, hospitalized							
SE-JH-H-A0006	67	F	Black	Non-Hispanic	90	NA	4LNC
SE-JH-H-A0026	50	M	Black	Non-Hispanic	104	NA	HFNC
SE-JH-H-A0077	57	M	White	Non-Hispanic	48	NA	Intubated
SE-JH-H-A0169	52	M	Other	Non-Hispanic	46	NA	2LNC
SE-JH-H-A0190	76	F	Black	Non-Hispanic	39	NA	Intubated
SE-JH-H-A0207	52	M	Black	Non-Hispanic	42	NA	HFNC
SE-JH-H-A0224	73	M	Other	Non-Hispanic	41	NA	Intubated
Median	57				46		

^APeak FLU-PRO score. ^BMaximum oxygen support required. 4LNC, 4 liters via nasal cannula; HFNC, high-flow oxygen via nasal cannula; intubated, requiring mechanical ventilation; 2LNC, 2 liters via nasal cannula.

(S-RBD-specific) B cells, and a cell surface phenotyping panel to characterize these cells. We focused on S-RBD-specific B cells because most virus-neutralizing human monoclonal antibodies target this domain (14–18). Neutralizing activity has been associated with protection against reinfection by other coronaviruses (19–22), and protection against challenge in animal models of SARS-CoV-2 infection (23, 24). Therefore, S-RBD-specific B cells are likely to be the cells responsible for production of protective neutralizing antibodies upon reexposure.

Classical markers applied to these S-RBD-specific B cells allowed us to identify B cell lineages including non-class-switched B cells, class-switched ASCs, class-switched resting (classical) MBCs (rMBCs), activated MBCs (actMBCs), atypical MBCs (atyMBCs), and intermediate MBCs (intMBCs). Additional subpopulations were identified by staining for a chemokine receptor (CXCR5) and potential inhibitory or activating receptors (FCRL5, CD22, and BTLA). Among the cell surface regulatory molecules, FCRL5 expression is of particular interest, since it is upregulated on long-lived antigen-specific rMBCs that develop after effective vaccination against influenza and tetanus (25, 26). This FCRL5⁺ rMBC population preferentially expands and forms plasmablasts on antigen rechallenge, indicating that FCRL5 expression on antigen-specific rMBCs is a marker of effective long-lived B cell-mediated immunity.

To investigate the potential for durable B cell immunity after SARS-CoV-2 infection, we analyzed S-RBD-specific B cells in ambulatory patients with COVID-19 with mild disease and hospitalized patients with moderate to severe disease. We detected S-RBD-specific non-class-switched B cells, S-RBD-specific class-switched ASCs, and/or S-RBD-specific class-switched MBCs in all participants, regardless of their serum antibody titers or disease severity. We analyzed the frequencies of these S-RBD-specific B

cell populations, and of S-RBD-specific MBC subsets, including rMBCs, intMBCs, actMBCs, and atyMBCs. By also quantifying cell surface molecules CD38, FCRL5, CD22, BTLA, and CXCR5 on these MBC populations and subsets, we identified a phenotypic profile of S-RBD-specific class-switched MBCs that was consistent with functional, durable B cell immunity.

Results

Selection of study participants. B cells were obtained from participants with mild COVID-19 disease, those with moderate to severe disease, and from healthy COVID-19-negative controls (Table 1). Participants with mild COVID-19 disease who never required hospitalization or supplemental oxygen were identified in a previously described cohort of ambulatory patients (27). Symptoms in this cohort were tracked using a FLU-PRO score calculated from a participant survey, as previously described (27). To ensure that participants with mild disease were included in this study, a group of 7 participants was selected with a median peak FLU-PRO score below the median peak score for the entire ambulatory cohort (FLU-PRO median of 0.09 [range 0.0–0.38] vs. 0.25 [0.0–1.63]). Seven additional participants with moderate to severe COVID-19 disease were selected from a second cohort of hospitalized patients (28), matched with the mild disease participants based on time since onset of symptoms at the time of blood sampling (median time since symptom onset in days: ambulatory = 61 [range 45–68]; hospitalized = 46 [range 39–104]). Peak supplemental oxygen support in hospitalized participants ranged from 2L via nasal cannula to mechanical ventilation. At the time of blood sampling for this study, 5 of the hospitalized participants had been discharged, and 2 remained hospitalized with critical illness. Hereafter, ambulatory, hospitalized, and healthy groups will be referred to as mild, severe, and healthy, respectively.

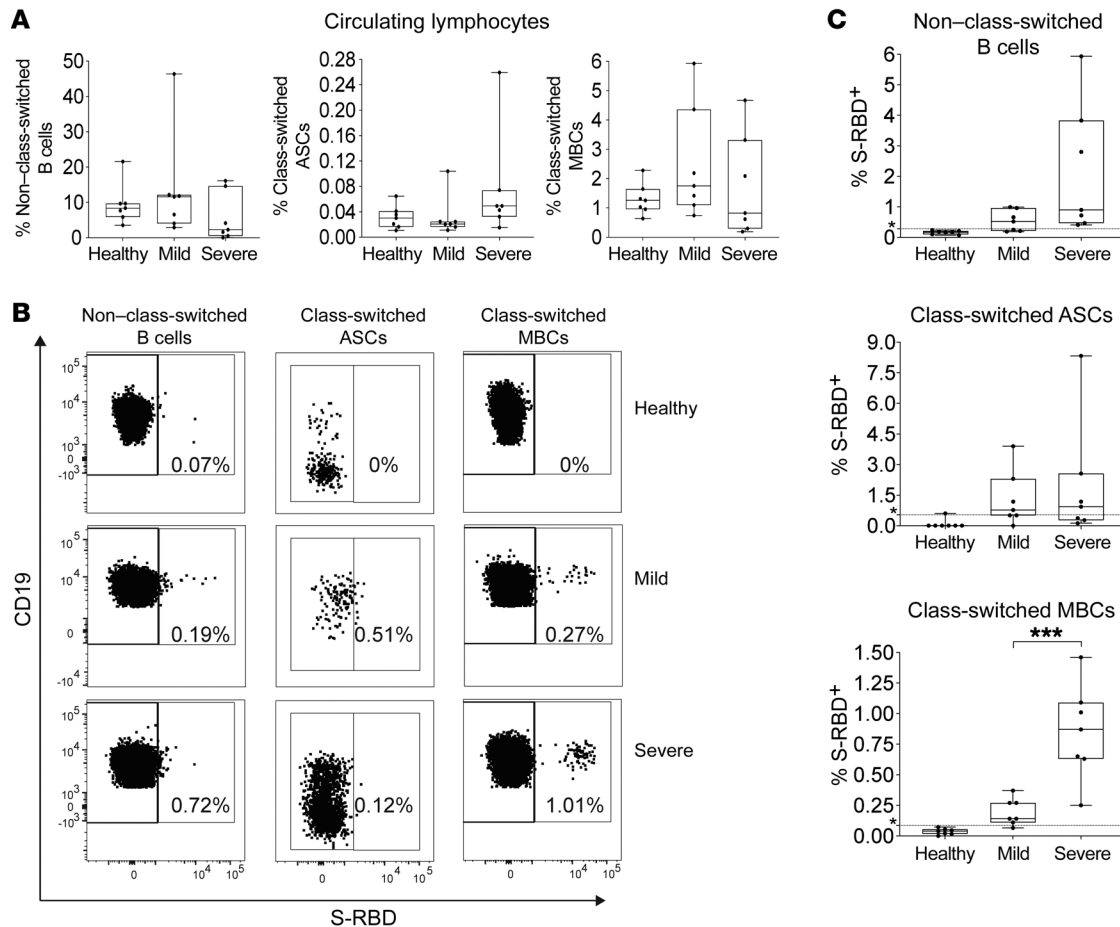


Figure 1. Quantifying S-RBD-specific B cells. (A) Percentage of lymphocytes that are class-switched MBCs, class-switched ASCs, or non-class switched B cells in healthy (COVID-19⁻), mild (COVID-19⁺, ambulatory), and severe (COVID-19⁺, hospitalized) participants (*n* = 7 for each group). (B) Gating strategy for S-RBD-specific non-class-switched B cells (CD3⁺, CD19⁺, IgD/IgM⁺, S-RBD⁺), S-RBD-specific class-switched MBCs (CD3⁺, CD19⁺, IgM⁻, IgD⁻, CD38^{+/-} (excluding ++), CD138⁻, S-RBD⁺), and S-RBD-specific class-switched ASCs (CD3⁺, CD19^{+/-}, IgM⁻, IgD⁻, CD38^{+/-}, CD27⁺, S-RBD⁺) in healthy, mild, and severe participants. (C) Percentage of class-switched MBCs, class-switched ASCs, and non-class-switched B cells that are S-RBD-specific in healthy, mild, and severe participants (*n* = 7 for each group). Dotted line represents the true positive threshold, defined as the mean plus 2 standard deviations of the healthy group. For box plots, horizontal lines indicate means, boxes are interquartile range, and whiskers are minimum to maximum. Normality of data was determined using Shapiro Wilk normality test. Comparisons in A were performed using 1-way ANOVA for normally distributed data or Kruskal-Wallis test for non-normally distributed data, with *P* values adjusted for multiple comparisons using the Benjamini, Krieger, and Yekutieli method. Comparisons between mild and severe patients in C were performed with 2-tailed *t* tests if data were normally distributed or Mann Whitney test if data were not normally distributed. Statistically significant comparisons are indicated (***) *P* ≤ 0.001.

Quantitation of S-RBD-specific B cells. A flow cytometry antibody panel was designed to identify non-class-switched B cells (CD3⁺, CD19⁺, IgD/IgM⁺), class-switched MBCs (CD3⁺, CD19⁺, IgM⁻, IgD⁻, CD38^{+/-} (excluding +/-), CD138⁻) and class-switched ASCs (CD3⁺, CD27⁺, CD19^{+/-}, IgM⁻, IgD⁻, CD38^{+/-}; Supplemental Figure 1; supplemental material available online with this article; <https://doi.org/10.1172/JCI145516DS1>). The frequency of all non-class-switched B cells, class-switched MBCs, or class-switched ASCs among single viable lymphocytes was not significantly different between healthy, mild, and severe groups, but there was a trend toward greater frequency of class-switched ASCs in the severe group compared with mild and healthy groups (Figure 1A).

As we defined these 3 B cell populations, we used a 6x-histidine (6xHis) tagged, soluble S-RBD protein followed by anti-His Alexa Fluor 647-conjugated antibody to stain cells expressing S-RBD-specific antibodies on their surface (Figure 1B and Supplemental

Figure 1). To confirm that the 6xHis-S-RBD staining was specific, we compared frequency of S-RBD⁺ class-switched MBCs measured using this protocol or by double staining with 2 different S-RBD proteins with 2 different tags (6xHis or mouse IgG1Fc; Supplemental Figure 2). We detected binding of these 2 S-RBD proteins to B cells using anti-HIS-Alexa 647 and anti-mouse Fc-PE antibodies, respectively. We observed nearly identical nonspecific background S-RBD⁺ frequency from a healthy donor using our standard 6xHis antigen alone or double staining (0.012% positive by standard protocol and 0.012% positive by double-staining protocol), and we also observed nearly identical S-RBD⁺ frequency from a patient with COVID-19 using our standard 6xHis antigen alone or double staining (0.64% positive by standard protocol and 0.61% positive by double-staining protocol, Supplemental Figure 2). Therefore, we performed all subsequent staining with a single 6xHis-S-RBD antigen. We quantitated the frequency of S-RBD-specific cells

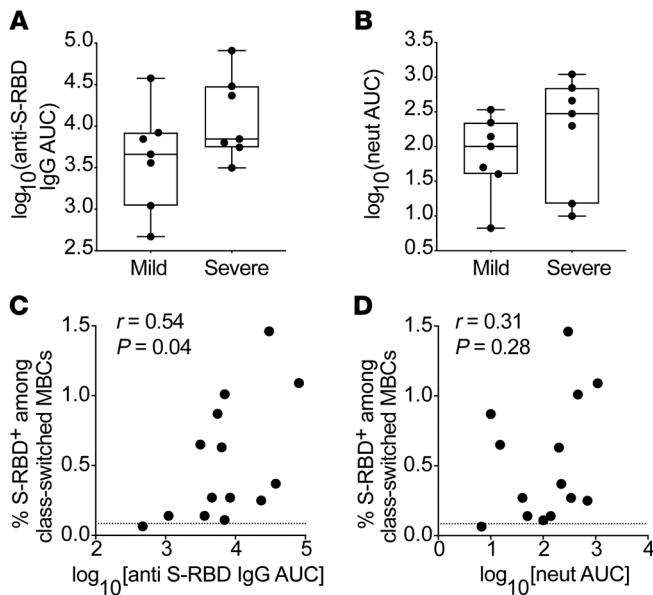


Figure 2. Comparisons of serum anti-S-RBD IgG and neutralizing antibody titers in mild and severe participants. (A) Anti S-RBD IgG AUC in mild or severe participants. **(B)** Neutralizing antibody AUC in mild or severe participants. **(C)** Correlation between percentage of class-switched MBCs that are S-RBD specific and plasma anti-S-RBD IgG AUC from the same subjects. **(D)** Correlation between percentage of class-switched MBCs that are S-RBD specific and plasma neutralizing antibody AUC values from the same subjects. Dotted line represents the true S-RBD positive threshold, defined as the mean plus 2 standard deviations of the healthy group. For box plots, horizontal lines indicate means, boxes are interquartile range, and whiskers are minimum to maximum. Normality of data was confirmed by Shapiro Wilk normality test. Significance in **A** and **B** was calculated using 2-tailed *t* tests. Correlation *r* and *P* values in **C** and **D** were calculated by the Pearson method.

among non-class-switched B cells, class-switched ASCs, and class-switched MBCs (Figure 1C). Four of 7 (57%) mild and 7 of 7 (100%) severe participants had a frequency of S-RBD-specific non-class-switched B cells above the true positive threshold set using the healthy group. The frequency of these cells did not differ significantly between the mild and severe groups. Since S-RBD specificity was detected by binding of S-RBD protein to cell surface immunoglobulin (Ig), detection of S-RBD-specific ASCs was limited to the subset of immature ASCs (plasmablasts) that had not yet down-regulated surface Ig expression. Four of 7 (57%) mild and 4 of 7 (57%) severe participants had a frequency of S-RBD-specific class-switched ASCs above the true positive threshold. The frequency of these cells also did not differ significantly between the mild and severe groups. Six of 7 (86%) mild and 7 of 7 (100%) severe participants had a frequency of S-RBD-specific class-switched MBCs above the true positive threshold. The single individual without detectable S-RBD-specific class-switched MBCs was asymptomatic throughout infection (peak FLU-PRO = 0.0). Frequency of S-RBD-specific class-switched MBCs was significantly higher in severe participants than in mild participants (mean S-RBD⁺ frequency 0.85% vs. 0.20%, *P* = 0.001). Taken together, these data demonstrate that S-RBD-specific cells could be detected among non-class-switched B cells and class-switched ASCs in most SARS-CoV-2-infected participants, and S-RBD-specific class-switched MBCs could be detected in 13 of 14 participants. S-RBD-specific cells were significantly more frequent among class-switched MBCs from the severe group relative to the mild group.

Detectable S-RBD-specific MBCs despite low levels of anti-S-RBD IgG and neutralizing antibodies in plasma. Given concerns that low or waning plasma titers of neutralizing antibodies in some individuals indicate a lack of a durable humoral response, we were interested in evaluating whether COVID-19 participants with low levels of plasma anti-S-RBD IgG and low neutralizing antibody levels had detectable S-RBD-specific MBCs in circulation. S-RBD binding IgG was measured using serial dilutions of plasma in an ELISA, and neutralizing antibodies were measured with serial dilutions of plasma in a micro-

neutralization assay using replication competent SARS-CoV-2 virus (10). Curves were fit to these data, and AUC values calculated. Anti-S-RBD IgG and neutralization AUC values each varied over a wide range across study subjects ($1 \times 10^{2.7} - 1 \times 10^{4.9}$ and $1 \times 10^{0.8} - 1 \times 10^{3.0}$, respectively). As expected based on prior studies (3, 10), there was a trend toward higher anti-S-RBD IgG and neutralization AUC values in the severe group relative to the mild group, although these differences were not statistically significant, likely due to the small number of subjects (Figure 2, A and B). We next evaluated whether there was a correlation between the frequency of S-RBD⁺ class-switched MBCs and levels of plasma anti-S-RBD IgG (Figure 2C) or levels of plasma neutralizing antibodies (Figure 2D). Notably, there was a significant correlation across all subjects between frequency of S-RBD⁺ class-switched MBCs and levels of plasma anti-S-RBD IgG (*r* = 0.54, *P* = 0.04). We did not observe a significant correlation between frequency of S-RBD⁺ class-switched MBCs and levels of neutralizing antibodies (*r* = 0.31, *P* = 0.28), possibly because only a subset of S-RBD⁺ MBCs are specific for neutralizing epitopes. The single individual without detectable S-RBD-specific class-switched MBCs had the lowest levels of plasma anti-S-RBD IgG (AUC = $1 \times 10^{2.7}$) and neutralizing antibodies (AUC = $1 \times 10^{0.8}$) in the study. Overall, these data show that S-RBD-specific class-switched MBCs were detectable in the circulation of most infected individuals, but that those with lower levels of plasma antibodies also showed lower frequency of S-RBD⁺ class-switched MBCs.

UMAP analysis of class-switched MBC surface markers. To further characterize the phenotypes of S-RBD-specific and non-specific class-switched MBCs in healthy, mild, or severe patients with COVID-19, we studied surface expression of CD21, CD27, FCRL5, CXCR5, CD22, BTLA, and CD38. For class-switched (IgM⁺, IgD⁻) MBCs, CD21 and CD27 expression allow identification of intMBCs (CD21⁺ CD27⁻), rMBCs (CD21⁺, CD27⁺), actMBCs (CD21⁻ CD27⁺), and atyMBCs (CD21⁻ CD27⁻) subsets. B and T lymphocyte attenuator (BTLA) or CD272 and CD22/Siglec2 are immune cell inhibitory receptors with cytoplasmic immunoreceptor tyrosine-based inhibition motifs (ITIMs) (29–32), while FCRL5 has 2 ITIMs and 1

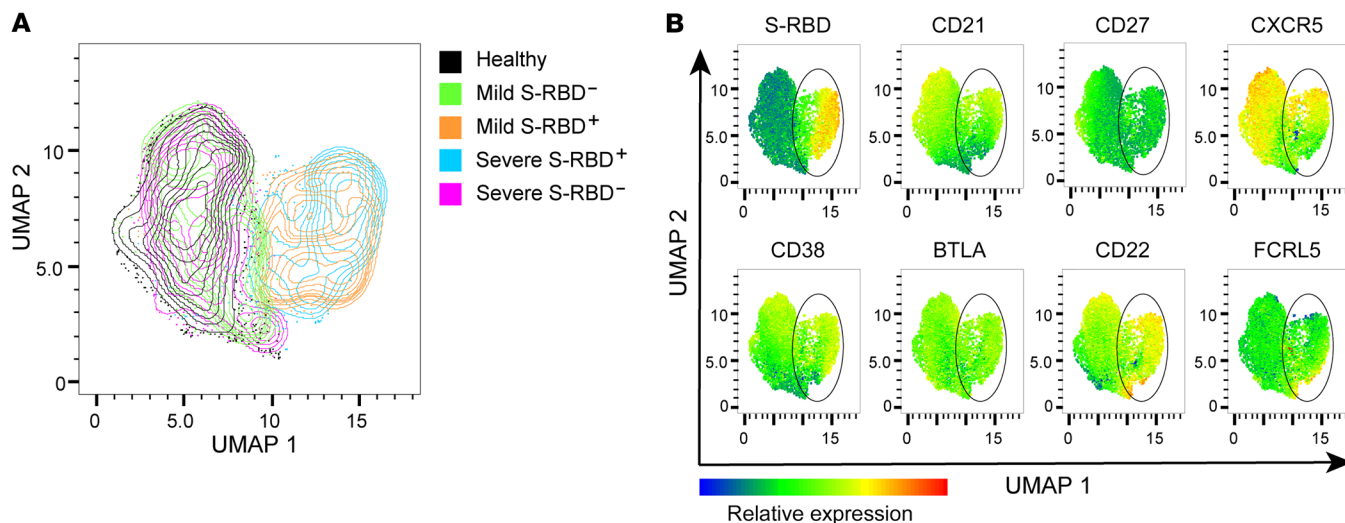


Figure 3. UMAP projection of class-switched MBCs and heatmap statistic of surface receptors. (A) Concatenated class-switched MBCs from healthy, mild, and severe subjects projected as a UMAP of S-RBD binding and CD21, CD27, CD38, FCRL5, CD22, CXCR5, and BTLA expression. All S-RBD⁺ MBCs were included, and S-RBD⁻ MBCs were downsampled to match S-RBD⁺ counts for each subject. (B) Multigraph color mapping of cell surface receptors on the UMAP projection, with S-RBD⁺ MBCs indicated on each UMAP with a black oval. Lowest expression is indicated by blue and highest expression by red.

immunoreceptor tyrosine-based activation motif (ITAM)(33, 34). CXC chemokine receptor type 5 (CXCR5) is a germinal center homing receptor that is useful, along with other surface markers, for differentiation of double-negative 1 (DN1) B cells, which are MBC precursors, from double-negative 2 (DN2) B cells, which are extrafollicular ASC precursors (35–37). CD38 expression varies across MBC subsets, and is typically low or negative on actMBCs, atyMBCs, and DN2 populations.

We first analyzed a UMAP projection of class-switched MBCs from healthy, mild, and severe groups generated based on binding of S-RBD and expression of CD21, CD27, CD38, CD22, FCRL5, CXCR5, and BTLA (Figure 3A). This UMAP showed a clear segregation of S-RBD⁺ cells from S-RBD⁻ cells. S-RBD⁺ cells from severe and mild patients were comingled, as were S-RBD⁻

cells from severe, mild, and healthy control groups. From this UMAP clustering projection, we extrapolated multigraph color mapping of the receptors showing a range of expression of all surface markers except BTLA (Figure 3B). CD22 and CD38 expression were greater in the S-RBD⁺ population than in the S-RBD⁻ cells from patients with COVID-19 or healthy donors. Notably, the S-RBD⁺ population also contained the cells with the highest and lowest levels of FCRL5 expression. To further analyze any differences between expression of these surface markers on all MBCs between severe or mild patients with COVID-19 and healthy donors, we generated a second UMAP that did not include S-RBD binding as a variable (Supplemental Figure 3). In this UMAP, there was no segregation of cells from severe, mild, or healthy donor groups, indicating that receptor expression was

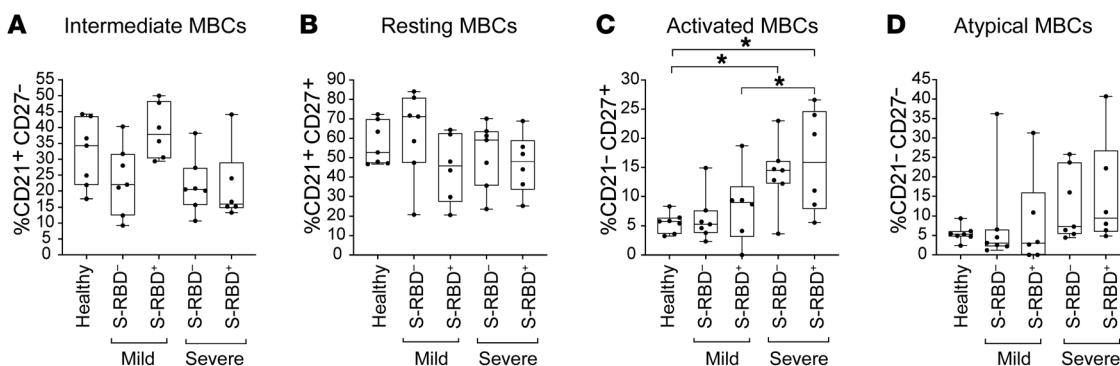


Figure 4. Frequency of MBC subsets in S-RBD⁻ or S-RBD⁺ class-switched MBCs from healthy, mild, or severe participants. Class-switched MBCs are defined as CD3⁺, CD19⁺, IgM⁻, IgD⁻, CD38^{+/−} (excluding ++), CD138⁻. In addition, (A) intMBCs are CD21⁺, CD27⁻; (B) rMBCs are CD21⁺, CD27⁻; (C) actMBCs are CD21⁺, CD27⁺; and (D) atyMBCs are CD21⁺, CD27⁺. Horizontal lines indicate means, boxes are interquartile range, and whiskers are minimum to maximum. Normality of data was determined using Shapiro Wilk normality test, and comparisons were performed using 1-way ANOVA for normally distributed data (B and C) or Kruskal-Wallis test for non-normally distributed data (A and D), with P values adjusted for multiple comparisons using the Benjamini, Krieger, and Yekutieli method. Statistically significant comparisons are indicated (* P ≤ 0.05).

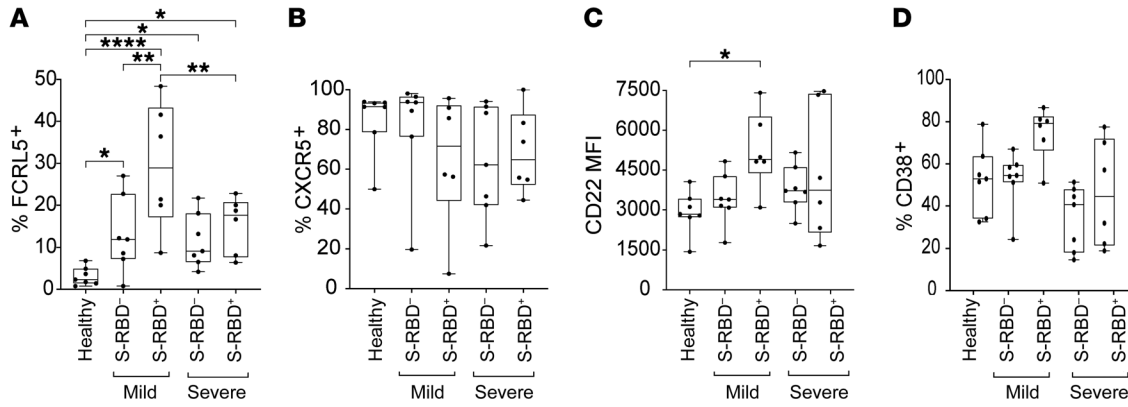


Figure 5. Surface expression of FcRL5, CXCR5, CD22, and CD38 on S-RBD⁻ or S-RBD⁺ class-switched MBCs from healthy, mild, or severe participants. Expression is shown as either percentage of cells positive or the MFI. (A) FcRL5, (B) CXCR5, (C) CD22, (D) CD38. Horizontal lines indicate means, boxes are interquartile range, and whiskers are minimum to maximum. Normality of data was determined using Shapiro Wilk normality test, and comparisons were performed using 1-way ANOVA for normally distributed data (A and C) or Kruskal-Wallis test for non-normally distributed data (B and D), with *P* values adjusted for multiple comparisons using the Benjamini, Krieger, and Yekutieli method. Statistically significant comparisons are indicated (**P* ≤ 0.05, ***P* ≤ 0.01, ****P* ≤ 0.001, *****P* ≤ 0.0001).

similar across all 3 groups. Overall, these UMAPs showed CD22 and CD38 upregulation in S-RBD⁺ MBCs, and a subset of S-RBD⁺ MBCs showed very high expression of FcRL5.

Quantifying subsets of S-RBD-nonspecific and S-RBD-specific class-switched MBCs. To better understand the functional phenotypes of the S-RBD-specific MBCs identified in both mild and severe groups, we compared the frequencies of intMBCs, rMBCs, actMBCs, and atyMBCs among S-RBD-specific and S-RBD-nonspecific class-switched MBCs at the level of individual participants (Figure 4). There were no statistically significant differences in frequencies of intMBCs, rMBCs, and atyMBCs (Figure 4, A-B, D). Class-switched (IgM⁺, IgD⁻) MBC subsets identified based on CD21 and CD27 expression have notably different phenotypes (38). Classical MBCs, also called rMBCs, persist for months to years and respond to antigen rechallenge by proliferating and differentiating into antibody-producing ASCs. ActMBCs are cells that recently left germinal centers and are already primed to become antibody secreting plasma cells (39). IntMBCs likely represent a transitional state between MBC subsets. AtyMBCs were

recently found to be more frequent among bulk (not antigen specific) MBCs during acute SARS-CoV-2 infection (40). AtyMBCs are also present at higher frequencies in chronic infections like HIV-1, hepatitis C virus, tuberculosis, or malaria, but their functional significance is unclear (41-43). They often express inhibitory receptors like FcRL4 (44), but they have also been shown to produce protective antibodies during malaria infection (43).

We detected medians of 69.5 absolute S-RBD-specific (range 1-454) and 13,971 S-RBD-nonspecific (range 152-84,645) class-switched MBCs for each participant. Only donors with more than 10 S-RBD-specific cells were included in subset analyses of S-RBD-specific MBCs, so subject A0046 (no detectable S-RBD-specific class-switched MBC frequency above background) and subject A0077 (severe lymphopenia) were excluded. S-RBD-nonspecific MBCs were adequately abundant in all participants to allow their inclusion in all analyses. There were no statistically significant differences in the frequencies of intMBCs, rMBCs, or atyMBCs subsets among S-RBD-specific or S-RBD-nonspecific class-switched MBCs from healthy, mild, or severe participants (Figure

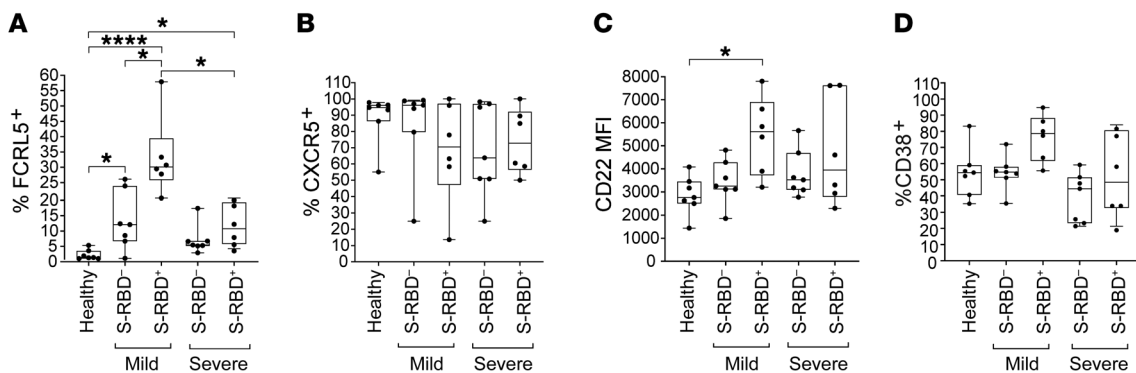


Figure 6. Surface expression of FcRL5, CXCR5, CD22, and CD38 on S-RBD⁺ class-switched rMBCs (CD21⁺, CD27⁺) from healthy, mild, or severe participants. Expression is shown as either percentage of cells positive or the MFI. (A) FcRL5, (B) CXCR5, (C) CD22, (D) CD38. Horizontal lines indicate means, boxes are interquartile range, and whiskers are minimum to maximum. Normality of data was determined using Shapiro Wilk normality test, and comparisons were performed using 1-way ANOVA for normally distributed data (C and D) or Kruskal-Wallis test for non-normally distributed data (A and B), with *P* values adjusted for multiple comparisons using the Benjamini, Krieger, and Yekutieli method. Statistically significant comparisons are indicated (**P* ≤ 0.05, *****P* ≤ 0.0001).

4). Although overall frequencies of atyMBCs did not differ between groups, we observed wide variation in the frequency of atyMBCs among S-RBD⁺ MBCs in the severe group. Notably, the 2 severe subjects with highest atyMBC frequency among S-RBD⁺ MBCs (A0190 and A0224) were also the 2 subjects who remained intubated at the time of analysis, whereas the other subjects in the severe group had recovered sufficiently to be discharged from the hospital. The third intubated severe patient, A077, was excluded from this analysis due to lymphopenia. In addition, actMBCs were significantly more frequent among both S-RBD⁻-nonspecific and S-RBD⁻-specific MBC populations in severe participants compared with healthy and mild participants (e.g., mean frequency of severe S-RBD⁺ MBCs vs. healthy S-RBD⁻ MBCs, 16.09% vs. 5.53%, $P = 0.01$; Figure 4C). This likely represents greater ongoing immune activation in the severe infection group relative to the healthy and mild groups and is also consistent with the observed trend toward higher frequency of ASCs in the severe group (Figure 1A). We observed a wide range in the frequency of S-RBD⁻-specific actMBCs, particularly among severe participants. There were no clear unifying clinical characteristics among the 3 severe subjects with highest frequencies of actMBCs among S-RBD⁺ MBCs (21%, 24%, and 27%), as their ages ranged from 52 to 76 years, days from onset of symptoms were near the median for the group (39–46 days), and maximum oxygen support ranged from 2L via nasal cannula to intubation.

We were also interested in evaluating the frequency of DN1 (IgD⁻, CD27⁻, CD21⁺, CXCR5⁺, FCRL5⁻) and DN2 (IgD⁻, CD27⁻, CD21⁻, CXCR5⁻, FCRL5⁺) populations among S-RBD⁺ and S-RBD⁻ B cells from healthy, mild, and severe groups, since DN1 cells are MBC precursors and DN2 cells are ASC precursors with an extra-follicular origin that often reach high frequency in the setting of active autoimmune disease (Supplemental Figure 4 and ref. 37). We observed no statistically significant differences between class-switched DN1 and DN2 frequencies among these different populations, although there was a trend toward greater DN2 frequency in both S-RBD⁻ and S-RBD⁺ cells from the severe group.

Overall, these data demonstrate an expected distribution of S-RBD⁻-specific cells among MBC subsets, with the largest proportion of S-RBD⁻-specific class-switched MBCs in both mild and severe groups falling in the rMBC (classical) subset.

Expression of activating or inhibitory surface markers on class-switched MBC and MBC subsets. To further investigate the differential expression of surface markers that we observed in the UMAP projections of grouped samples, we compared expression of FCRL5, CXCR5, CD22, and CD38 at the level of individual participants between healthy, mild S-RBD⁻, mild S-RBD⁺, severe S-RBD⁻, and severe S-RBD⁺ groups (Figure 5). BTLA expression was not included in this analysis given no differential expression in the UMAP. We found that FCRL5 was dramatically upregulated in mild S-RBD⁺ MBCs relative to healthy cells, mild S-RBD⁻ cells, and severe S-RBD⁺ cells ($P < 0.0001$, 0.003, and 0.01, respectively). FCRL5 was also upregulated to a lesser, but still significant extent on severe S-RBD⁺, mild S-RBD⁻, and severe S-RBD⁻ MBCs relative to healthy MBCs ($P = 0.01$, 0.03, and 0.04, respectively, Figure 5A). The frequency of CXCR5⁺ cells among class-switched MBCs was not significantly different between the groups (Figure 5B). Since CD22/siglec-2 is ubiquitously expressed on B cells, we analyzed its relative expression by comparing mean fluorescence

intensities (MFIs). Compared with healthy controls, CD22 was upregulated on mild S-RBD⁺ class-switched MBCs ($P = 0.04$; Figure 5C), which was consistent with upregulation of CD22 in the S-RBD⁺ population in the UMAP analysis. Among class-switched MBCs, CD38 expression did not differ significantly between SARS-CoV-2 infected and healthy participants (Figure 5D), although there was a trend toward greater expression of CD38 on mild S-RBD⁺ class-switched MBCs, which was consistent with upregulation in the S-RBD⁺ population in the UMAP analysis.

Having observed significant upregulation of both FCRL5 and CD22, and a trend toward upregulation of CD38 on S-RBD⁺ class-switched MBCs, we analyzed expression of surface markers on MBC subsets rMBCs, intMBCs, actMBCs, and atyMBCs (Figure 6 and Supplemental Figure 5). As with total class-switched S-RBD⁺ MBCs, we found that FCRL5 was dramatically upregulated on mild S-RBD⁺ rMBCs relative to healthy rMBCs, mild S-RBD⁻ rMBCs, and severe S-RBD⁺ rMBCs ($P < 0.0001$, 0.038, and 0.038, respectively). FCRL5 was also upregulated to a lesser, but still significant extent on severe S-RBD⁺ and mild S-RBD⁻ rMBCs relative to healthy rMBCs ($P = 0.017$ and 0.017, respectively, Figure 6A). As shown in Supplemental Figure 5, CXCR5 was significantly downregulated on mild S-RBD⁺ atyMBCs relative to healthy atyMBCs, mild S-RBD⁻ atyMBCs, and severe S-RBD⁺ atyMBCs ($P = 0.003$, 0.020, and 0.009, respectively). CD22 was significantly upregulated on mild S-RBD⁺ rMBCs and intMBCs relative to healthy cells ($P = 0.020$ and 0.033, respectively, Figure 6C and Supplemental Figure 5C). Frequencies of CD38⁺ and CXCR5⁺ cells were not significantly different between the groups (Figure 6, B and D). CD38⁺ cells were not significantly different between the groups. Taken together, these results indicate that FCRL5 was significantly upregulated on S-RBD⁻-specific rMBCs in both mild and severe infection. In mild but not severe infection, CD22 was upregulated on S-RBD⁻-specific rMBCs and intMBCs, and CXCR5 was downregulated on S-RBD⁻-specific atyMBCs.

Discussion

To investigate the durability of B cell immunity after SARS-CoV-2 infection, we analyzed S-RBD⁻-specific B cells in ambulatory patients with COVID-19 with mild disease and hospitalized patients with moderate to severe disease, at a median of 54 days after onset of symptoms. We detected S-RBD⁻-specific class-switched MBCs in 13 of 14 participants, failing only in the individual with lowest plasma levels of anti-S-RBD IgG and neutralizing antibodies. We saw a significant correlation between frequency of S-RBD⁺ class-switched MBCs and plasma anti-S-RBD IgG levels across all participants, indicating that individuals with lower plasma antibody titers may also mount less robust anti-S-RBD MBC responses. The largest proportion of S-RBD⁻-specific class-switched MBCs in both cohorts were rMBCs. AtymBCs were a minor population. FCRL5 was upregulated on S-RBD⁻-specific rMBCs after severe infection, and upregulated even more dramatically after mild infection.

These findings are of particular interest given the observation of Kaneko, et al. of a dramatic loss of germinal centers in lymph nodes and spleens after SARS-CoV-2 infection (13). This observation would suggest that SARS-CoV-2-specific B cells in infected individuals lack T cell help and would therefore have reduced capacity to

undergo class switching and transition to a resting memory phenotype. Our data indicate that despite this loss of germinal centers, T cell help is adequate to facilitate class switching of S-RBD-specific B cells, and transition of many of these cells to a resting state, regardless of disease severity. These data support prior studies, which also found that the majority of S-RBD-specific B cells in individuals who had recovered from COVID-19 showed a resting memory phenotype (45, 46). We did not measure the extent of somatic hypermutation of these B cells, but multiple groups have already demonstrated that human S-RBD-specific antibodies acquire enough somatic mutations to achieve very high affinity (14–18), again demonstrating that T cell help is adequate in most individuals.

A prior study by Oliviero et al. of bulk (not antigen-specific) MBC subsets during acute or convalescent COVID-19 found that atyMBCs were expanded during acute infection, with atyMBC frequencies normalizing during convalescence (40). Our study extends that evaluation by studying both S-RBD-specific and S-RBD-nonspecific MBCs. We found that S-RBD-specific and S-RBD-nonspecific atyMBCs, DN1, and DN2 frequencies did not differ significantly from healthy controls, but S-RBD-specific and S-RBD-nonspecific actMBCs were expanded in severely infected individuals. This observation of increased frequency of actMBCs in severe disease might be explained by studies demonstrating greater activation of T cells, including CD4⁺ T follicular helper cells, in severe COVID-19 disease (47, 48). The contrast of our results with those of Oliviero et al. likely arise from differing timing after infection, and also by our focus on antigen-specific MBCs. The fact that frequencies of atyMBCs, DN1, and DN2 B cells frequencies do not differ from healthy controls provides further evidence that S-RBD-specific MBC response is probably normally functional.

It is interesting that the single individual without detectable S-RBD-specific class-switched MBCs was asymptomatic throughout infection, and also had the lowest levels of anti-S-RBD IgG and neutralizing antibodies in the study. Given the low frequency of S-RBD-specific MBCs across the cohort, we would need to analyze a larger number of PBMCs to confirm with confidence that this individual is truly negative for S-RBD-specific class-switched MBCs. We also saw a significant correlation between frequency of S-RBD⁺ class-switched MBCs and plasma anti-S-RBD IgG levels across all participants, indicating that individuals with relatively lower plasma antibody titers may also mount relatively less robust anti-S-RBD MBC responses.

A limitation of this study is the lack of long-term longitudinal sampling of B cells after infection, which would be required to prove that the S-RBD-specific MBC responses observed here are truly durable. These studies will be pursued as longitudinal samples become available. Additionally, we analyzed low numbers of S-RBD-specific class-switched MBCs in some subjects due to low frequency and a limitation of available PBMCs, so phenotyping of MBC subsets should be interpreted with some caution. However, we have shown here that S-RBD-specific MBCs in most infected individuals have a phenotype that very closely resembles the phenotype of germinal center-derived MBCs induced by effective vaccination against influenza and tetanus. Indeed, this observation is supported by 2 very recent studies with longitudinal B cell sampling after COVID-19 infection, demonstrating that S-RBD-specific B cell frequencies were stable or increasing over time (46, 49).

Of particular note in this study is the upregulation of FCRL5 on S-RBD-specific class-switched rMBCs after either mild or severe disease. FCRL5 is expressed by most germinal center-derived MBCs in plasmodium-infected mice, and these FCRL5⁺ MBCs differentiate into ASCs on rechallenge (25). In addition, Kim et al. found that in humans, presumably vaccinated against tetanus months to years prior, FCRL5 was upregulated on tetanus-specific rMBCs (CD21⁺, CD27⁺) but not on bulk rMBCs (25). Nellore et al. showed similar results after influenza vaccination of humans, demonstrating that HA-specific FCRL5⁺ MBCs were induced by vaccination, and that these FCRL5⁺ MBCs preferentially differentiated into plasmablasts upon antigen rechallenge approximately a year after vaccination (26). Although FCRL5 was upregulated on S-RBD-specific rMBCs in both mild and severe disease, it was upregulated to a greater extent in mild disease. This may reflect a more typical MBC response in mild disease, and a more dysfunctional response in severe disease. Further longitudinal studies are needed to compare persistence and expansion after antigen rechallenge of rMBCs with very high versus more modest FCRL5 expression. Further studies will be also necessary to understand the implications of CD22 upregulation on S-RBD-specific rMBCs and intMBCs, CXCR5 downregulation on S-RBD-specific atyMBCs, and a trend toward CD38 upregulation on S-RBD-specific rMBCs and actMBCs. The functions of CXCR5 and CD38 in this context are unclear, but we would speculate that since CD22 is an inhibitory receptor, expression may help to maintain MBCs in a resting state, which could favor long-term persistence of S-RBD-specific MBCs. Overall, despite our lack of longitudinal testing, the phenotypic similarity of S-RBD-specific MBCs in this study to typical, germinal center-derived MBCs induced by effective vaccination provide strong evidence that these S-RBD-specific MBCs are durable and functional.

In summary, we have demonstrated that S-RBD-specific class-switched MBCs develop in most SARS-CoV-2-infected individuals, including those with mild disease or low levels of plasma anti-S-RBD IgG and neutralizing antibodies. The most abundant subset of S-RBD-specific class-switched MBCs in both cohorts were rMBCs, and atyMBCs were a minor population. FCRL5, a marker of a functional memory response when expressed on antigen-specific rMBCs, was dramatically upregulated on S-RBD-specific rMBCs, particularly after mild infection. These data indicate that most SARS-CoV-2-infected individuals develop S-RBD-specific, class-switched MBCs that phenotypically resemble B cells induced by effective vaccination against other pathogens, providing evidence for durable humoral immunity against SARS-CoV-2 after recovery from either mild or severe COVID-19. These data have implications for risk of reinfection after recovery from COVID-19, and also provide a standard against which B cell responses to novel SARS-CoV-2 vaccines could be compared.

Methods

Study participants

Participants with mild COVID-19 who never required hospitalization or supplemental oxygen were identified in a cohort of ambulatory COVID-19 patients. Symptoms in this cohort were tracked using a FLU-PRO score calculated from a participant survey, as previously

described (27). Participants with moderate to severe COVID-19 were selected from a cohort of hospitalized patients (28), and matched with the mild participants based on time since onset of symptoms at the time of blood sampling. PBMCs cryopreserved prior to the onset of the COVID-19 pandemic were also obtained from anonymous healthy blood donors. Healthy and COVID-19 participant blood specimens were ficoll gradient separated into plasma and PBMCs. PBMCs were viably cryopreserved in FBS plus 10% DMSO for future use.

Expression and purification of soluble S-RBD

Plasmid preparation. Recombinant plasmid constructs containing modified S-RBD and a beta-lactamase (amp) gene were obtained (50) and amplified in *E. coli* after transformation and growth on LB agar plates coated with ampicillin. The plasmids were extracted using GigaPrep kits (Thermo Fisher Scientific) and eluted in molecular biology grade water.

Recombinant protein expression. HEK293.2sus cells (ATCC) were obtained and adapted to Freestyle F-17 medium (Thermo Fisher Scientific) and BalanCD (Irvine Scientific) using polycarbonate shake flasks (Fisherbrand) with 4 mM GlutaMAX supplementation (Thermo Fisher Scientific). The cells were routinely maintained every 4 days at a seeding density of 0.5 million cells/mL. They were cultured at 37°C, 90% humidity with 5% CO₂ for cells in BalanCD, whereas those in F-17 were maintained at 8% CO₂. Cells were counted using trypan blue dye (Gibco) exclusion method and a hemocytometer. Cell viability was always maintained above 90%. Twenty-four hours prior to transfection (day -1), the cells were seeded at a density of 1 million cells/mL, ensuring that the cell viability was above 90%. Polyethylenimine (PEI) stocks with 25 kDa molecular mass (Polysciences) were prepared in MilliQ water at a concentration of 1 mg/mL. This was filter sterilized through a 0.22 µm syringe filter (Corning), aliquoted, and stored at -20°C. On the day of transfection (day 0), the cells were counted to ensure sufficient growth and viability. OptiPRO SFM (Gibco) was used as the medium for transfection mixture. For 100 mL of cell culture, 2 tubes were aliquoted with 6.7 mL each of OptiPRO, one for PEI and the other for rDNA. A DNA/PEI ratio of 1:3.5 was used for transfection. A volume of 350 µL prepared PEI stock solution was added to tube 1 while 100 µg rDNA was added to tube 2 and incubated for 5 minutes. After incubation, these were mixed together, incubated for 10 minutes at room temperature, and then added to the culture through gravity addition. The cells were returned back to the 37°C incubator. A day after transfection (day 1), the cells were spun down at 400g for 7 minutes at room temperature and resuspended in fresh media with GlutaMAX supplementation. Three to 5 hours after resuspension, 0.22 µm sterile filtered sodium butyrate (EMD Millipore) was added to the flask at a final concentration of 5 mM (51). The cells were allowed to grow for a period of 4 to 5 days. Cell counts, viability, and glucose and lactate values were measured every day. Cells were harvested when either the viability fell below 60% or when the glucose was depleted by centrifugation at 900g for 10 minutes at room temperature. Cell culture supernatants containing either recombinant S-RBD or S protein were filtered through 0.22 µm PES membrane stericup filters (MilliporeSigma) to remove cell debris and stored at -20°C until purification.

Protein purification. Protein purification by immobilized metal affinity chromatography (IMAC) and gravity flow was adapted from previous methods (23). After washing with PBS (Thermo Fisher Scientific), nickel-nitrilotriacetic acid (Ni-NTA) agarose (Qiagen) was added

to culture supernatant followed by overnight incubation (12–16 hours) at 4°C on a rotator. For every 150 mL of culture supernatant, 2.5 mL of Ni-NTA agarose was added. The 5 mL gravity flow polypropylene columns (Qiagen) were equilibrated with PBS. One polypropylene column was used for every 150 mL of culture supernatant. The supernatant-agarose mixture was loaded onto the column to retain the agarose beads with recombinant proteins bound to the beads. Each column was then washed, first with 1× culture supernatant volume of PBS and then with 25 mL of 20 mM imidazole (MilliporeSigma) in PBS wash buffer to remove host cell proteins. Recombinant proteins were then eluted from each column in 3 fractions with 5 mL of 250 mM imidazole in PBS elution buffer per fraction, giving a total of 15 mL eluate per column. The eluate was subsequently dialyzed several times against PBS using Amicon Ultra Centrifugal Filters (MilliporeSigma) at 7000 rpm for 20 minutes at 10°C to remove the imidazole and concentrate the eluate. Filters with a 10 kDa molecular weight cut-off were used for S-RBD eluate. The final concentration of the recombinant S-RBD and S proteins was measured by bicinchoninic acid (BCA) assay (Thermo Fisher Scientific), and purity was assessed on 10% SDS-PAGE (Bio-Rad) followed by Coomassie blue staining. After sufficient destaining in water overnight, clear single bands were visible for S-RBD.

Viruses and cells. Vero-E6 cells (ATCC CRL-1586) and Vero-E6-TMPRSS2 cells (24) were cultured in Dulbecco's modified Eagle medium (DMEM) containing 10% fetal bovine serum (Gibco), 1 mM glutamine (Invitrogen), 1 mM sodium pyruvate (Invitrogen), 100 U/mL penicillin (Invitrogen), and 100 µg/mL streptomycin (Invitrogen) (complete media [CM]). Cells were incubated in a 5% CO₂ humidified incubator at 37°C. The SARS-CoV-2/USA-WA1/2020 virus was obtained from BEI Resources. The infectious virus titer was determined on Vero cells using a 50% tissue culture infectious dose (TCID₅₀) assay as previously described for SARS-CoV (25, 26). Serial 10-fold dilutions of the virus stock were made in infection media (IM, which is identical to CM except the FBS is reduced to 2.5%), then 100 µL of each dilution was added to Vero cells in a 96-well plate in sextuplicate. The cells were incubated at 37°C for 4 days, visualized by staining with naphthol blue-black, and scored visually for cytopathic effect. A Reed and Muench calculation was used to determine TCID₅₀ per milliliter (27).

Measurement of endpoint anti-S-RBD IgG titer

The protocol was adapted from a published protocol from Florian Krammer's laboratory (50). Ninety-six well plates (Immulon 4HBX, Thermo Fisher Scientific) were coated with S-RBD at a volume of 50 µL of 2 µg/mL diluted antigen in filtered, sterile 1× PBS (Thermo Fisher Scientific) at 4°C overnight. Coating buffer was removed, plates were washed 3 times with 300 µL PBS-T wash buffer (1× PBS plus 0.1% Tween 20, Thermo Fisher Scientific), and blocked with 200 µL PBS-T with 3% nonfat milk (milk powder, American Bio) by volume for 1 hour at room temperature. All plasma samples were heat inactivated at 56°C on a heating block for 1 hour prior to use. Negative control samples were prepared at 1:10 dilutions in PBS-T in 1% nonfat milk and plated at a final concentration of 1:100. A monoclonal antibody (mAb) specific for the SARS-CoV-2 spike protein was used as a positive control (1:5000, Sino Biological). For serial dilutions of plasma on S-RBD-coated plates, plasma samples were prepared in 3-fold serial dilutions starting at 1:20 in PBST in 1% nonfat milk. Blocking solution was removed and 10 µL diluted plasma was added in dupli-

cate to plates and incubated at room temperature for 2 hours. Plates were washed 3 times with PBS-T wash buffer and 50 μ L secondary antibody was added to plates and incubated at room temperature for 1 hour. Anti-human secondary antibodies used included Fc-specific total IgG HRP (1:5000 dilution, Invitrogen), prepared in PBS-T plus 1% nonfat milk. Plates were washed and all residual liquid removed before adding 100 μ L SIGMAFAST OPD (o-phenylenediamine dihydrochloride) solution (Sigma Aldrich) to each well, followed by incubation in darkness at room temperature for 10 minutes. To stop the reaction, 50 μ L of 3M hydrochloric acid (HCl, Thermo Fisher Scientific) was added to each well. The OD of each plate was read at 490 nm (OD 490) on a SpectraMax i3 ELISA plate reader (BioTek). The positive cutoff value for each plate was calculated by summing the average of the negative values and 3 times the standard deviation of the negatives. All values at or above the cutoff value were considered positive. Values were graphed on a dose response curve, a best fit line drawn by nonlinear regression, and AUC calculated.

Measurement of endpoint neutralization titer

Plasma neutralization titers were determined as described for SARS-CoV (52). Two-fold dilutions of plasma (starting at a 1:20 dilution) were made in IM. Infectious virus was added to the plasma dilutions at a final concentration of 1×10^4 TCID₅₀/mL (100 TCID₅₀ per 100 μ L). The samples were incubated for 1 hour at room temperature, then 100 μ L of each dilution was added to 1 well of a 96-well plate of VeroE6-TMPRSS2 cells in sextuplet for 6 hours at 37°C. The inoculums were removed, fresh IM was added, and the plates were incubated at 37°C for 2 days. The cells were fixed by the addition of 150 μ L of 4% formaldehyde per well, incubated for at least 4 hours at room temperature, then stained with naphthol blue-black. The nAb titer was calculated as the highest serum dilution that eliminated cytopathic effect (CPE) in 50% of the wells. Values were graphed on a dose response curve, a best fit line drawn by nonlinear regression, and AUC calculated.

Cell staining and flow cytometry

PBMCs were isolated from blood using ficoll separation gradient and viably frozen. Cells were thawed before use, and $5 \times 10^6 - 10 \times 10^6$ PBMCs were stained from each participant. Fc blocker (Becton Dickinson, catalog 564220) diluted in FACS buffer (1x PBS with 1% BSA) was added to the cells and incubated for 30 minutes on ice or at 4°C. The cells were then washed twice with FACS buffer. Soluble 6x-His tagged S-RBD protein was then added to the cells and incubated at room temperature for 30 minutes. This was followed by wash steps with FACS buffer. Conjugated antibodies (Supplemental Table 1 for list of antibodies and their conjugate fluorophores) and live dead stain were then added to the cells and incubated for an additional 30 minutes. The cells were washed 2 or 3 more times before running the cells on BD Biosciences LSR II instrument.

There were $1 \times 10^6 - 6 \times 10^6$ total events collected for each participant, resulting in medians of 69.5 absolute S-RBD⁺ and 13,971 S-RBD⁻ class-switched MBCs for each participant (ranges 1–454 S-RBD⁺, 152–84,645 S-RBD⁻ MBCs). All S-RBD⁺ MBCs from all study subjects ($n = 1600$) were included in each UMAP. To allow clear visualization of both S-RBD⁺ and S-RBD⁻ cells in the Figure 3 UMAP, S-RBD⁻ cells were downsampled for each subject to match the number of S-RBD⁺ cells from that subject. For Supplemental Figure 3, S-RBD⁻ cells were downsampled to 3000 cells per subject to maximize the number of

cells analyzed while equalizing the input from each subject. The subject with only 1 S-RBD⁺ cell was excluded from S-RBD⁺ MBC subset analyses. Positive gates for each fluorophore were set after compensation and using fluorescence minus one (FMO) staining and isotype control antibodies. Representative FCRL5 staining is shown in Supplemental Figure 6.

Confirmation of specificity of S-RBD staining

For double staining with 2 different S-RBD proteins (Supplemental Figure 2), a similar staining protocol was used with the inclusion of S-RBD, mouse IgG1 Fc, Avitag (MALS verified) protein from AcroBioSystems (Thermo Fisher Scientific, catalog 50-201-9394). Binding of this protein was detected with PE anti-mouse IgG1 antibody (Supplemental Table 1). BTLA, CD22, FCRL5, and CXCR5 were not stained in this experiment.

Statistics

FlowJo software was used to analyze all the flow results from the LSRII. Statistical analyses were performed in Prism (Graphpad software). Two group comparisons were performed with 2-sided *t* tests if data were normally distributed based on Shapiro Wilk normality test or Mann Whitney rank test if data were not normally distributed. Multigroup comparisons were performed using 1-way ANOVA if data were normally distributed based on Shapiro Wilk normality test or Kruskal-Wallis test if data were not normally distributed, with *P* values adjusted for multiple comparisons using the Benjamini, Krieger, and Yekutieli method. Adjusted *P* values less than 0.05 were considered significant.

Study approval

This research was approved by the Johns Hopkins University School of Medicine IRB. Prior to blood collection, all participants provided informed written consent.

Author contributions

COO conceived the project, performed experiments, interpreted data, and wrote the initial manuscript draft. NES conceived the project, performed experiments, and interpreted data. PWB, AARA, and SCR interpreted data. HSP, KL, AG, SD, AP, and SLK performed experiments and interpreted data. PL and MJB provided reagents. YCM conceived the project and provided participant samples. ALC conceived the project, provided participant samples, and interpreted data. JRB conceived the project, interpreted data, and wrote the initial manuscript draft. All authors reviewed and edited the manuscript.

Acknowledgments

We would like to thank participants in the study, Florian Krammer for providing the S-RBD plasmid, and members of the Johns Hopkins Viral Hepatitis Center for thoughtful discussion. We thank the Bloomberg Flow Cytometry and Immunology Core for equipment and technical assistance. We thank the National Institute of Infectious Diseases, Japan, for providing VeroE6TMPRSS2 cells. We acknowledge the Centers for Disease Control and Prevention, BEI Resources, NIAID, NIH for SARS-related coronavirus 2, isolate USA-WA1/2020, NR-5228. This research was supported by the National Institutes of Health grants R01AI127469 and

R21AI151353 (to JRB), U54CA260492 (SLK and AC), and in part by the NIH Center of Excellence for Influenza Research and Surveillance (HHSN272201400007C to AP and SLK).

Address correspondence to: Justin R. Bailey, 855 N. Wolfe Street, Rangos Building, Suite 520, Baltimore, Maryland 21205, USA. Phone: 410.614.6087; Email: jbailey7@jhmi.edu.

- Guan WJ, Zhong NS. Clinical characteristics of Covid-19 in China. Reply. *N Engl J Med*. 2020;382(19):1861-1862.
- Wang Z, et al. Clinical features of 69 cases with Coronavirus disease 2019 in Wuhan, China. *Clin Infect Dis*. 2020;71(15):769-777.
- Long QX, et al. Antibody responses to SARS-CoV-2 in patients with COVID-19. *Nat Med*. 2020;26(6):845-848.
- Seow J, et al. Longitudinal evaluation and decline of antibody responses in SARS-CoV-2 infection [preprint]. <https://doi.org/10.1101/2020.07.09.20148429>. Posted on medRxiv July 11, 2020.
- Ibarrondo FJ, et al. Rapid decay of anti-SARS-CoV-2 antibodies in persons with Mild Covid-19. *N Engl J Med*. 2020;383(11):1085-1087.
- Patel MM, et al. Change in antibodies to SARS-CoV-2 over 60 days among health care personnel in Nashville, Tennessee. *JAMA*. 2020;324(17):1781-1782.
- Wajnberg A, et al. SARS-CoV-2 infection induces robust, neutralizing antibody responses that are stable for at least three months [preprint]. <https://doi.org/10.1101/2020.07.14.20151126>. Posted on medRxiv July 17, 2020.
- Isho B, et al. Persistence of serum and saliva antibody responses to SARS-CoV-2 spike antigens in COVID-19 patients. *Sci Immunol*. 2020;5(52):eabe5511.
- Iyer AS, et al. Persistence and decay of human antibody responses to the receptor binding domain of SARS-CoV-2 spike protein in COVID-19 patients. *Sci Immunol*. 2020;5(52):eabe0367.
- Klein SL, et al. Sex, age, and hospitalization drive antibody responses in a COVID-19 convalescent plasma donor population. *J Clin Invest*. 2020;130(11):6141-6150.
- Salimzadeh L, et al. PD-1 blockade partially recovers dysfunctional virus-specific B cells in chronic hepatitis B infection. *J Clin Invest*. 2018;128(10):4573-4587.
- Middleman AB, et al. Duration of protection after infant hepatitis B vaccination series. *Pediatrics*. 2014;133(6):e1500-e1507.
- Kaneko N, et al. Loss of Bcl-6-expressing T follicular helper cells and germinal centers in COVID-19. *Cell*. 2020;183(1):143-157.
- Robbiani DF, et al. Convergent antibody responses to SARS-CoV-2 in convalescent individuals. *Nature*. 2020;584(7821):437-442.
- Zost SJ, et al. Potently neutralizing and protective human antibodies against SARS-CoV-2. *Nature*. 2020;584(7821):443-449.
- Noy-Porat T, et al. A panel of human neutralizing mAbs targeting SARS-CoV-2 spike at multiple epitopes. *Nat Commun*. 2020;11(1):4303.
- Rogers TF, et al. Isolation of potent SARS-CoV-2 neutralizing antibodies and protection from disease in a small animal model. *Science*. 2020;369(6506):956-963.
- Brouwer PJM, et al. Potent neutralizing antibodies from COVID-19 patients define multiple targets of vulnerability. *Science*. 2020;369(6504):643-650.
- Buchholz UJ, et al. Contributions of the structural proteins of severe acute respiratory syndrome coronavirus to protective immunity. *Proc Natl Acad Sci U S A*. 2004;101(26):9804-9809.
- Du L, et al. The spike protein of SARS-CoV-2 a target for vaccine and therapeutic development. *Nat Rev Microbiol*. 2009;7(3):226-236.
- Li T, et al. Long-term persistence of robust antibody and cytotoxic T cell responses in recovered patients infected with SARS coronavirus. *PLoS One*. 2006;1:e24.
- Huang AT, et al. A systematic review of antibody mediated immunity to coronaviruses: antibody kinetics, correlates of protection, and association of antibody responses with severity of disease. *Nat Commun*. 2020;11(1):4704.
- Deng W, et al. Primary exposure to SARS-CoV-2 protects against reinfection in rhesus macaques. *Science*. 2020;369(6505):818-823.
- Chandrashekar A, et al. SARS-CoV-2 infection protects against challenge in rhesus macaques. *Science*. 2020;369(6505):812-817.
- Kim CC, et al. FCRL5⁺ memory B cells exhibit robust recall responses. *Cell Rep*. 2019;27(5):1446-1460.
- Nellore A, et al. Fcrl5 and T-bet define influenza-specific memory B cells that predict long-lived antibody responses [preprint]. <https://doi.org/10.1101/643973>. Posted on bioRxiv May 20, 2019.
- Blair PW, et al. The clinical course of COVID-19 in the outpatient setting: a prospective cohort study. *Open Forum Infect Dis*. 2021;8(2):ofab007.
- Thompson EA, et al. Metabolic programs define dysfunctional immune responses in severe COVID-19 patients [preprint]. <https://doi.org/10.1101/2020.09.10.20186064>. Posted on medRxiv October 05, 2020.
- Crocker PR, et al. Siglecs and their roles in the immune system. *Nat Rev Immunol*. 2007;7(4):255-266.
- Macauley MS, et al. Siglec-mediated regulation of immune cell function in disease. *Nat Rev Immunol*. 2014;14(10):653-666.
- Tateno H, et al. Distinct endocytic mechanisms of CD22 (Siglec-2) and Siglec-F reflect roles in cell signaling and innate immunity. *Mol Cell Biol*. 2007;27(16):5699-5710.
- Watanabe N, et al. BTLA is a lymphocyte inhibitory receptor with similarities to CTLA-4 and PD-1. *Nat Immunol*. 2003;4(7):670-679.
- Davis RS. FCRL regulation in innate-like B cells. *Ann N Y Acad Sci*. 2015;1362(1):110-116.
- Liao HX, et al. Co-evolution of a broadly neutralizing HIV-1 antibody and founder virus. *Nature*. 2013;496(7446):469-476.
- Hardtke S, et al. Balanced expression of CXCR5 and CCR7 on follicular T helper cells determines their transient positioning to lymph node follicles and is essential for efficient B-cell help. *Blood*. 2005;106(6):1924-1931.
- Junt T, et al. CXCR5-dependent seeding of follicular niches by B and Th cells augments antiviral B cell responses. *J Immunol*. 2005;175(11):7109-7116.
- Sanz I, et al. Challenges and opportunities for consistent classification of human B cell and plasma cell populations. *Front Immunol*. 2019;10:2458.
- Sanz I, et al. Phenotypic and functional heterogeneity of human memory B cells. *Semin Immunol*. 2008;20(1):67-82.
- Lau D, et al. Low CD21 expression defines a population of recent germinal center graduates primed for plasma cell differentiation. *Sci Immunol*. 2017;2(7):eaai8153.
- Oliviero B, et al. Expansion of atypical memory B cells is a prominent feature of COVID-19. *Cell Mol Immunol*. 2020;17(10):1101-1103.
- Moir S, et al. Evidence for HIV-associated B cell exhaustion in a dysfunctional memory B cell compartment in HIV-infected viremic individuals. *J Exp Med*. 2008;205(8):1797-1805.
- Joosten SA, et al. Patients with tuberculosis have a dysfunctional circulating B-cell compartment, which normalizes following successful treatment. *PLoS Pathog*. 2016;12(6):e1005687.
- Muellenbeck MF, et al. Atypical and classical memory B cells produce Plasmodium falciparum neutralizing antibodies. *J Exp Med*. 2013;210(2):389-399.
- Sohn HW, et al. FcRL4 acts as an adaptive to innate molecular switch dampening BCR signaling and enhancing TLR signaling. *Blood*. 2011;118(24):6332-6341.
- Juno JA, et al. Humoral and circulating follicular helper T cell responses in recovered patients with COVID-19. *Nat Med*. 2020;26(9):1428-1434.
- Rodda LB, et al. Functional SARS-CoV-2-specific immune memory persists after mild COVID-19. *Cell*. 2020;184(1):169-183.
- Kuri-Cervantes L, et al. Comprehensive mapping of immune perturbations associated with severe COVID-19. *Sci Immunol*. 2020;5(49):eabd7114.
- Chen Z, John Wherry E. T cell responses in patients with COVID-19. *Nat Rev Immunol*. 2020;20(9):529-536.
- Dan JM, et al. Immunological memory to SARS-CoV-2 assessed for up to 8 months after infection. *Science*. 2021;371(6529):eabf4063.
- Stadlbauer D, et al. SARS-CoV-2 Seroconversion in Humans: A Detailed Protocol for a Serological Assay, Antigen Production, and Test Setup. *Curr Protoc Microbiol*. 2020;57(1):e100.
- Grünberg J, et al. High-yield production of recombinant antibody fragments in HEK-293 cells using sodium butyrate. *Biotechniques*. 2003;34(5):968-972.
- Schaecher SR, et al. An immunosuppressed Syrian golden hamster model for SARS-CoV infection. *Virology*. 2008;380(2):312-321.